PHYSICAL REVIEW B VOLUME 26, NUMBER 9 1 NOVEMBER 1982

Transient grating investigation of exciton diffusion and fluorescence quenching in $Nd_xLa_{1-x}P_5O_{14}$ crystals

Christopher M. Lawson and Richard C. Powell
Physics Department, Oklahoma State University, Stillwater, Oklahoma 74078

Walter K. Zwicker
Philips Laboratories, Briarcliff Manor, New York 10510

(Received 29 March 1982; revised manuscript received 15 June 1982)

The use of degenerate four-wave-mixing techniques to investigate exciton migration in highly concentrated laser materials is discussed. A theoretical derivation is presented of the signal beam intensity for this technique using the geometric arrangement common for energy-transfer studies. The results demonstrate effects that occur when the pump beams are not exactly phase matched and the instabilities encountered for very small pump-beam-crossing angles. Applying this technique to crystals of $Nd_xLa_{1-x}P_5O_{14}$ shows that exciton diffusion takes place in a given direction with diffusion lengths between 0.18 and 0.36 μm for samples with x ranging from 0.2 to 1.0, respectively. Fluorescence quenching is shown to vary linearly with concentration at high values of x and quadratically at low values of x. This is consistent with an exciton migration and trapping mechanism at high concentrations and cross relaxation at low concentrations.

I. INTRODUCTION

We report here the results of an investigation of the properties of exciton diffusion in $Nd_xLa_{1-x}P_5O_{14}$ crystals using degenerate four-wave-mixing (FWM) techniques. Preliminary results of this work were given in Ref. 1. This paper presents a detailed derivation of some of the theoretical aspects of FWM, as well as extending the experimental data to an additional mixed crystal with a different composition and discussing the relevance of these results to the understanding of the concentration quenching characteristics of this material.

Investigating the optical properties of the so called "stoichiometric rare-earth laser materials" has been a topic of great interest in recent years, due to their possible important applications as "mini-lasers."[2,3] Understanding the concentration quenching in these materials is of specific interest since it is quite different from other rare-earth laser materials. Past work involving both site-selection spectroscopy[4] and fluorescent line narrowing spectroscopy[5] has shown that at low temperatures spectral diffusion of energy does not take place. However, spatial migration of energy has been observed over long distances at room temperature,[1] and the details of this process are described here. These measurements were made by degenerate FWM spectroscopy techniques in which an excited-state population grating is established and probed by chopped laser excitation. This form of transient grating spectroscopy has been shown to be an important method of determining exciton diffusion lengths in organic solids,[6] and has the important property of being able to detect spatial migration of energy without spectral diffusion.

Although the theory of FWM has been developed by several authors,[6-12] the form of the expression describing the scattering efficency is different depending on the specific experimental orientation used. In Sec. III a derivation is presented of the FWM scattering efficiency expression assuming the experimental arrangement important for exciton migration studies. Several aspects of this expression are discussed which have not previously been addressed in other theoretical treatments. In Sec. IV the experimental results obtained from FWM measurements on $Nd_xLa_{1-x}P_5O_{14}$ crystals are discussed and the properties of concentration quenching in this type of material are investigated.

II. SAMPLES AND EXPERIMENTAL APPARATUS

Large size single crystals of high optical quality $Nd_xLa_{1-x}P_5O_{14}$ were grown by the previously described flux technique from hot phosphoric

acid.[13] The crystals grown were greater than 4 cm in cross section, which allowed samples of various crystallographic orientations to be cut and polished. The three samples studied had fractional concentrations of Nd^{3+} of $x=0.2$, $x=0.6$, $x=1.0$.

The experimental configuration used for this work is shown in Fig. 1. The 5145-Å line of an argon laser was used because it falls on the edge of one of the absorption bands of Nd^{3+}. The beam is sent through a 1-m focal length lens and then split into three beams. The weak probe beam (labeled *p* in the figure) is split off using a variable beam splitter. The two pump beams (labeled *a* and *b* in the figure) are split off using a 50-50 beam splitter. The path lengths of the pump beams must be within the coherence length of the laser, but the probe beam path length is purposely made much different to discourage gratings formed through the interference of the probe beam with one of the pump beams. The probe beam is aligned counterpropagating to pump beam *b*. This probe beam is then Bragg diffracted off the interference grating formed by the interaction of two pump beams in the sample so that the diffracted signal beam (label *s*) counterpropagates back along pump beam *a*. The signal beam is then picked off using a beam splitter and directed into a photomultiplier tube. To analyze the transient behavior of the grating decay both of the pump beams are mechanically chopped, and the decay of the signal beam is monitored using a boxcar integrator and *x-y* recorder. The optics are slightly misaligned to prevent feedback into the laser. In addition, various orientations of polarizers have been used to decrease background light levels and an LSI-11 computer system has been used to analyze the data.

The laser directly pumps a Nd^{3+} absorption band

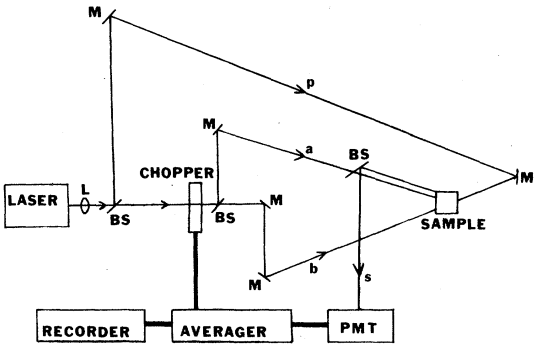

FIG. 1. Experimental configuration for transient grating measurements. Beams *a* and *b* are the pump beams, beam *p* is the probe beam, and beam *s* is the signal beam.

made up of overlapping $^2G_{9/2}$ and $^4G_{7/2}$ levels. There is then rapid radiationless relaxation to the $^4F_{3/2}$ metastable state from which the fluorescence emission occurs to the various components of the ^4I ground state term. The excited-state relaxation occurs on a time scale too rapid to be detected by this experiment. The energy migration occurs while the ions are in the metastable state, and it is the diffusion coefficient of this mobile excited state which is measured by this experiment.

III. THEORY

The theory of FWM has recently been addressed in several papers[6–12] using two fundamentally different approaches. References 6 and 8 model the system as the probe beam Bragg diffracting off of a sinusoidally varying complex index of refraction grating. This is useful in studying the physical processes that destroy the grating in time. This is especially important in exciton-migration studies, and the results of this theory will be used in Sec. IV to analyze experimental data. References 7, 9, and 10 model the system by explicitly considering the nonlinear wave equations where the electric fields are coupled by the nonlinear susceptibility in the material. Furthermore, Refs. 9 and 10 consider the mechanisms creating this nonlinear susceptibility by modeling the system as an ensemble of two- and three-level atoms, respectively. This approach yields important information about the steady-state scattering efficiency. In interpreting FWM data it is important to understand the signal properties as fully as possible, and thus in discussing the results in Sec. IV theoretical predictions of both approaches are utilized. The Bragg scattering approach is used to directly determine information on exciton diffusion,[6,11] and the nonlinear interaction model is used to explain the dependence of signal strength and stability on alignment characteristics. Previous work with the latter model assumed phase-matched, counterpropagating pump beams. The FWM scattering efficiency is rederived below, modeling the media as a two-level system as in Ref. 9 but including important extensions to the theory consistent with the configuration used for exciton-migration studies. It is recognized that this treatment using interacting plane waves in a two-level system must be considered only a rough approximation to the real case of focused Gaussian beams[8] in a multilevel system (Nd^{3+}). However, the general features of the signal intensity predicted by the simplified model are still useful in understanding the

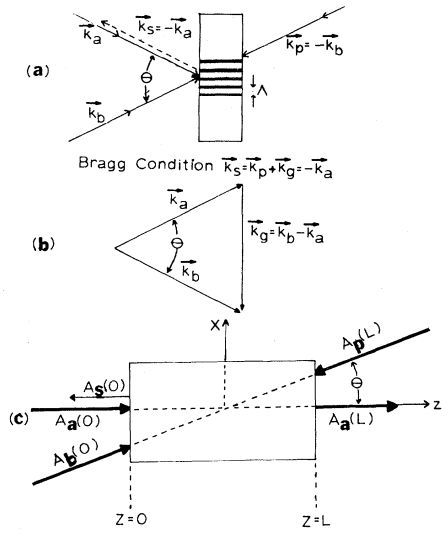

FIG. 2. (a) Grating formation geometry. (b) Conservation of wave vector and the Bragg condition. (c) Sample and electric field geometry.

observed signal properties. No attempt is made to relate these results to specific material properties since important properties such as dispersion in the excited state are not included in this simple model.

In the FWM configuration generally used to study energy migration, a laser beam is split into two strong "pump" beams of wave vectors $\vec{k}_a$ and $\vec{k}_b$, and a weaker "probe" beam of wave vector $\vec{k}_p$ which counterpropagates against one of the pump beams. This is shown in Fig. 2. The two pump beams interfere in the medium and optical absorption by the active ions creates a spatial distribution of excited states with a sinusoidal pattern of wave vector $\vec{k}_g=\vec{k}_b-\vec{k}_a$. Corresponding to the grating wave vector $\vec{k}_g$ is the grating wavelength given by $\Lambda=\lambda/(2\sin\theta/2)$, where λ is the laser wave length and θ is the crossing angle of the two pump beams. The depth of the grating can then be ascertained by Bragg diffraction of the probe beam. With the probe beam counterpropagating against the pump beam which has wave vector $\vec{k}_b$, the Bragg condition requires the scattered signal beam to have wave vector $\vec{k}_s=\vec{k}_p+\vec{k}_g=-\vec{k}_a$, which implies that the signal beam counterpropagates back against the pump beam with wave vector $\vec{k}_a$ (see Fig. 2).

The assumptions will be made that all beams are linearly polarized in the same direction, with the pump beam electric field given by $E_b(\vec{r},t)$ and $E_a(\vec{r},t)$, the probe field as $E_p(\vec{r},t)$, and the signal beam as $E_s(\vec{r},t)$. If the z axis is taken to be along the pump beam with electric field E_a, then the configuration will be as shown in Fig. 2 which is similar to the geometry of Refs. 7 and 9. By making the "parametric approximation" that the pump beams are undepleted in the media, then the four electric fields are given as

$$E_p(\vec{r},t)=A_p(z)e^{i\omega t}e^{-\vec{k}_p\cdot\vec{r}},$$
$$E_s(\vec{r},t)=A_s(z)e^{i\omega t}e^{-\vec{k}_s\cdot\vec{r}},$$
$$E_b(\vec{r},t)=A_b e^{i\omega t}e^{i\vec{k}_p\cdot\vec{r}},$$
$$E_a(\vec{r},t)=A_a e^{i\omega t}e^{i\vec{k}_s\cdot\vec{r}}.$$

The wave equation that these fields must obey in the material is

$$\nabla^2 E-\epsilon_0\mu_0\frac{\partial^2 E}{\partial t^2}=\mu_0\frac{\partial^2 P}{\partial t^2}, \tag{1}$$

where ϵ_0 is the permitivity constant, μ_0 is the permeability constant, and P is the polarization. The polarization P may be expressed in terms of the susceptibility as

$$P(E)=\epsilon_0\chi(E)E. \tag{2}$$

The media can be modeled as two-level system with the susceptibility given by[9,14]

$$\chi(E)=-\frac{2\alpha_0}{k}\left[\frac{i+\delta}{1+\delta^2+|E/E_S|^2}\right], \tag{3}$$

where δ is the normalized detuning from line center, $|E_s|^2$ is the saturation intensity, and α_0 is the line center small-signal field attenuation coefficient. The total pump-beam electric field $E_0=E_a+E_b$ will have a much larger amplitude than the sum of the electric fields of the probe beam and the signal beam $\Delta E=E_p+E_s$. Thus the polarization can be expanded to first order in $\Delta E/E_0$ to obtain[9]

$$P(E_0+\Delta E)=e^{i\omega t}\epsilon_0\chi(E_0)\left[E_0+\Delta E-\frac{(E_0^2\Delta E^*+|E_0|\Delta^2 E)}{I_S+|E_0|^2}\right], \tag{4}$$

where $I_S=|E_S|^2(1+\delta^2)$.

With the use of the slowly varying envelope approximation, $|\partial^2 A_i/\partial z^2| \ll |k_i\partial A_i/\partial z|$, $i=p,s$, Eq. (1) becomes

$$2ike^{i\omega t}\left[\cos\theta e^{-i\vec{k}_p\cdot\vec{r}}\frac{\partial A_p(z)}{\partial z}+e^{-i\vec{k}_s\cdot\vec{r}}\frac{\partial A_s(z)}{\partial z}\right]=-k^2e^{i\omega t}\chi(E_0)\left[E_0+\Delta E-\frac{(E_0^2\Delta E^*+|E_0|^2\Delta E)}{I_S+|E_0|^2}\right], \tag{5}$$

where $k^2=|\vec{k}_p|^2=|\vec{k}_s|^2$.

The only terms of interest on the right-hand side are those that satisfy the phase matching condition, i.e. those terms that synchronously drive the left-hand side as either $\exp[i(\omega t-\vec{k}_s\cdot\vec{r})]$ or $\exp[i(\omega t-\vec{k}_p\cdot\vec{r})]$. Defining the pump-beam intensities as $I_b=|A_b|^2$ and $I_a=|A_a|^2$, Eq. (5) becomes

$$\left[\cos\theta e^{-i\vec{k}_p\cdot\vec{r}}\frac{\partial A_p(z)}{\partial z}+e^{-i\vec{k}_s\cdot\vec{r}}\frac{\partial A_s(z)}{\partial z}\right]=\frac{\alpha_0|E_s|^2(1-i\delta)}{(I_S+|E_0|^2)^2}$$

$$\begin{aligned}=&((I_S+|E_0|^2)(A_pe^{-i\vec{k}_p\cdot\vec{r}}+A_se^{-i\vec{k}_s\cdot\vec{r}})\\&-(I_b+I_a)(A_pe^{-i\vec{k}_p\cdot\vec{r}}+A_se^{-i\vec{k}_s\cdot\vec{r}})-A_pA_bA_a^*e^{-i\vec{k}_s\cdot\vec{r}}\\&-A_sA_b^*A_ae^{-i\vec{k}_p\cdot\vec{r}}-\{A_b^*A_a\exp[-i(\vec{k}_p-\vec{k}_s)\cdot r]\}A_pe^{-i\vec{k}_p\cdot\vec{r}}\\&-\{A_bA_a^*\exp[i(\vec{k}_p-\vec{k}_s)\cdot\vec{r}]\}A_se^{-i\vec{k}_s\cdot\vec{r}}).\end{aligned} \tag{6}$$

The phase mismatch Δ of the two pump beams is given by $\Delta=\phi_b-\phi_a$, where $A_b=|A_b|\exp(i\phi_b)$ and $A_a=|A_a|\exp(i\phi_a)$. Since the signal beam is much weaker than the probe beam for this type of FWM experiment, Eq. (6) leads to two coupled wave equations. Along the z axis, these are

$$\frac{\partial A_p(z)}{\partial z}+p(z)A_p(z)=0, \tag{7}$$

$$\frac{\partial A_s(z)}{\partial z}+P(z)A_s(z)=Q(z), \tag{8}$$

where

$$p(z)=\frac{-\alpha_0|E_S|^2(1-i\delta)}{\cos\theta}\left\{\frac{I_S+|A_bA_a|\exp\{+i[k(1-\cos\theta)z+\Delta]\}}{\{I_S+I_b+I_a+2|A_bA_a|\cos[k(1-\cos\theta)z+\Delta]\}^2}\right\},$$

$$P(z)=-\alpha_0|E_S|^2(1-i\delta)\left\{\frac{I_S+|A_bA_a|\exp\{-i[k(1-\cos\theta)z+\Delta]\}}{\{I_S+I_b+I_a+2|A_bA_a|\cos[k(1-\cos\theta)z+\Delta]\}^2}\right\},$$

and

$$Q(z)=\frac{-\alpha_0|E_S|^2(1-i\delta)|A_bA_a|e^{i\Delta}A_p(z)}{\{I_S+I_b+I_a+2|A_bA_a|\cos[k(1-\cos\theta)z+\Delta]\}^2}.$$

It can be seen that $p(z)$, $P(z)$, and $Q(z)$ each oscillate with z with oscillation wavelength $\lambda_{os}=\lambda/(1-\cos\theta)$. The solutions to Eqs. (7) and (8) fall into two categories, depending on whether or not $p(z)$, $P(z)$, and $Q(z)$ oscillate rapidly over distances where $A_p(z)$ and $A_s(z)$ change appreciably. These will be treated separately.

Case I: θ is not small

If θ is not small, then $A_p(z)$ and $A_s(z)$ do not change appreciably over λ_{os}. Since $p(z)$, $P(z)$, and $Q(z)$ then oscillate many times over distances where $A_p(z)$ and $A_s(z)$ change appreciably, they may be averaged over an oscillation wavelength. The solution to Eq. (7) is then

$$A_p(z)=A_p(L)\exp[\xi\sec\theta(z-L)]\ , \tag{9}$$

where $A_p(L)$ is the incident probe-beam amplitude and ξ is the complex absorption coefficient given by

$$\xi=\frac{\alpha_0(1-i\delta)}{(1+\delta^2)}\left[\frac{1+(I_b/I_S)+(I_a/I_S)-2I_bI_a/I_S^2}{\{[1+(I_b/I_S)+(I_a/I_S)]^2-4I_bI_a/I_S^2\}^{3/2}}\right]. \tag{10}$$

With the use of the boundary condition that there is no incident signal beam, i.e., $A_s(0)=0$, the solution to Eq. (8) is

$$A_s(z)=-\frac{-A_p(L)}{\sec\theta-1}\left[\frac{|A_bA_a|e^{i\Delta}}{I_S}\left[\frac{[1+(I_b+I_a)/I_S]}{[1+(I_b+I_a)/I_S-2I_bI_a/I_S^2]}\right]\right]$$

$$\times\{\exp[\xi\sec\theta(z-L)]-\exp[\xi(z-L)]\}\ . \tag{11}$$

One quantity of interest is the signal-beam intensity as it exits the sample $|A_s(0)|^2$, since this is an experimentally measureable quantity,

$$|A_s(0)|^2=\frac{(I_bI_a/I_S)[1+(I_b/I_S)+(I_a/I_S)]^2}{[1+(I_b/I_S)+(I_a/I_S)-2I_bI_a/I_S^2]^2}[|A_p(L)|^2/(\sec\theta-1)^2]$$

$$\times\{\exp(-2\xi_RL)+\exp(-2\xi_R\sec\theta L)-2\exp[-\xi_R(1+\sec\theta)L]\cos[\xi_i(1-\sec\theta)L]\}\ , \tag{12}$$

where ξ_R and ξ_i are the real and imaginary parts of Eq. (10), respectively. Normally in a degenerate FWM experiment the two pump beams and the probe beam are obtained by splitting one laser beam into three parts. When this is the case, one sees from Eq. (12) that the output signal-beam intensity will vary as the cube of the laser power.

A good measure of the "scattering efficiency" η of the FWM processes is the ratio of the exciting signal beam $|A_s(0)|^2$ to the exiting probe beam in the absence of the pump-beam interactions. With the use of Eqs. (9) and (10), we have

$$|A_p(0)|^2_{E_0=0}=|A_p(L)|^2\exp\{-[2\alpha_0/(1+\delta^2)]L\}\ .$$

The scattering efficiency η is then given by

$$\eta=\frac{(I_bI_a/I_S^2)[1+(I_b/I_S)+(I_a/I_S)]^2}{\{[1+(I_b/I_S)+(I_a/I_S)]-2I_bI_a/I_S^2\}^2}\frac{\exp[2\alpha_0L/(1+\delta^2)]}{(\sec\theta-1)^2}$$

$$\times\{\exp(-2\xi_RL)+\exp(-2\xi_R\sec\theta L)-2\exp[-\xi_R(1+\sec\theta)L]\cos[\xi_i(1-\sec\theta)L]\}\ . \tag{13}$$

The dependence of the scattering efficiency on crossing angle can be clarified somewhat whenever $|\xi L(1-\sec\theta)|$ is small. This will usually be true since the experiment does not work well if

(i) $|\xi L|$ is large since the beams are than essentially extinguished in the crystal.

(ii) θ is very large since the output signal-beam intensity decreases with increasing θ.

Thus under this condition, to first order in $|\xi L(1-\sec\theta)|$, Eq. (13) becomes

$$\eta=\frac{\alpha_0^2}{1+\delta^2}\left[\frac{(I_bI_a/I_S^2)[1+(I_b+I_a)/I_S]^2L^2\exp(-2\xi_RL)\exp[2\alpha_0L/(1+\delta^2)]}{\{[1+(I_b+I_a)/I_S]^2-4I_bI_a/I_S^2\}^3}[1+\xi_RL(1-\sec\theta)]\right]. \tag{14}$$

Equation (14) shows that the scattering efficiency decreases strongly with increasing crossing angle θ.

Whenever the pump intensity is well below the saturation intensity, to lowest order in $(I_b+I_a)/I_S$ the scattering efficiency reduces to

$$\eta=\frac{\alpha_0^2L^2}{1+\delta^2}(I_bI_a/I_S^2)\left[1+\frac{\alpha_0L}{1+\delta^2}(1-\sec\theta)\right]. \tag{15}$$

Experimentally, one usually works with crossing angles large enough that case I applies and Eqs. (13), (14), or (15) will be applicable. However, it is of interest to derive the expression for scattering efficiency for very small crossing angles in certain limiting cases to discover what new effects should be expected in this situation.

Case II: θ is small

If θ is very small, then $A_p(z)$ and $A_s(z)$ do change appreciably over λ_{os}. Equations (7) and (8) cannot be solved exactly in this case. However, they can be solved approximately whenever the pump beams are well below saturation intensity.

Defining α as

$$\alpha=\frac{\alpha_0(i-i\delta)}{(1+\delta^2)}[1+(I_b+I_a)/I_S]^{-2},$$

the output intensity of the signal beam can be formed from the solution of Eqs. (7) and (8) (Ref. 15) to first order in $|A_bA_a|/I_S$,

$$\begin{aligned}|A_s(0)|^2=L|\alpha|^2\frac{I_bI_a}{I_S^2}|A_p(L)|^2e^{-2\alpha_RL}\\ \times\left\{L+\frac{2|A_bA_a|L}{k(1-\cos\theta)I_S}\{3\alpha_R\sin[k(1-\cos\theta)L+\Delta]-\alpha_i\cos[k(1-\cos\theta)L+\Delta]\}\right.\\ -\frac{12|A_bA_a|\alpha_R}{k^2(1-\cos\theta)^2I_S}\sin\left[\frac{k(1-\cos\theta)L}{2}+\Delta\right]\sin\left[\frac{k(1-\cos\theta)L}{2}\right]\\ \left.-\frac{4|A_bA_a|}{k(1-\cos\theta)I_S}\left[4-\frac{\alpha_i}{k(1-\cos\theta)}\right]\left[\sin\left[\frac{k(1-\cos\theta)L}{2}\right]\cos\left[\frac{k(1-\cos\theta)L}{2}+\Delta\right]\right]\right\}.\end{aligned} \tag{16}$$

The scattering efficiency is then

$$\begin{aligned}\eta=L|\alpha|^2(I_bI_a/I_S^2)\exp[2\alpha_0L/(1+\delta^2)]\exp(-2\alpha_RL)\\ \times\left\{L+\frac{2|A_bA_a|L}{k(1-\cos\theta)I_S}\{3\alpha_R\sin[k(1-\cos\theta)L+\Delta]-\alpha_i\cos[k(1-\cos\theta)L+\Delta]\}\right.\\ -\frac{12|A_bA_a|\alpha_R}{k^2(1-\cos\theta)^2I_S}\sin\left[\frac{k(1-\cos\theta)L}{2}+\Delta\right]\sin\left[\frac{k(1-\cos\theta)L}{2}\right]\\ \left.-\frac{4|A_bA_a|}{k(1-\cos\theta)I_S}\left[4-\frac{\alpha_i}{k(1-\cos\theta)}\right]\left[\sin\left[\frac{k(1-\cos\theta)L}{2}\right]\cos\left[\frac{k(1-\cos\theta)L}{2}+\Delta\right]\right]\right\}.\end{aligned} \tag{17}$$

Important information about the type of effects expected at small crossings angles can be obtained by examining Eqs. (16) and (17). One can see that all of the terms that are first order in $|A_bA_a|/I_S$ vary sinusoidally with the phase mismatch Δ of the two pump beams. If the pump beams are within the coherence length of each other, then $\Delta=(2\pi/\lambda)\Delta L$ where ΔL is the difference in path length. All terms that are first order in $|A_bA_a|/I_S$ will therefore be exceptionally sensitive to vibrations and to precise alignment of the pump beams. Thus at very small angles, Eqs. (16) and (17) predict the observed signal beam to have a component that oscillates very rapidly due to vibrations or minor adjustments superimposed on an "envelope signal" that is insensitive to vibrations and precise alignments. The observation of this type of behavior is discussed in the following section.

IV. EXPERIMENTAL RESULTS AND INTERPRETATION

Information about spatial energy migration in $Nd_xLa_{1-x}P_5O_{14}$ crystals at room temperature was obtained using the FWM configuration described previously and observing the decay of the Bragg diffracted signal beam. Useful data was obtained

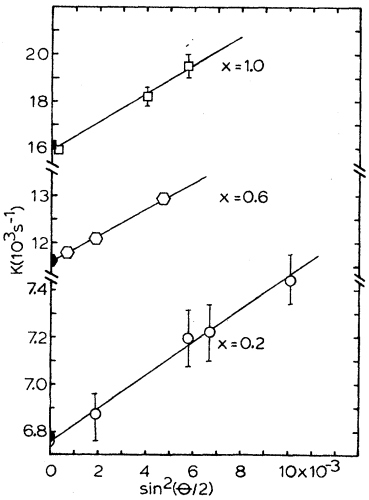

FIG. 3. Variation of grating decay constant with the square of the sine of half the pump-beam crossing angle at room temperature. The shaded points are twice the fluorescence decay rates.

only for $\theta \geq 2°$ since the signal beam was found to be extremely unstable at smaller crossing angles. The signal had two components at these small angles. One component was exceptionally sensitive to vibrations and to the exact alignment of the experiment, and underwent many oscillations whenever slight alignment changes were made. This component was superimposed on another much stabler component. This small-angle behavior is exactly what is predicted by Eqs. (16) and (17).

Whenever the pump beams are chopped and the grating is destroyed by fluorescence decay and exciton diffusion, the signal beam is predicted to decay exponentially with decay constant K given by[6,11]

$$K=(32\pi^2 D/\lambda^2)\sin^2(\theta/2)+2/\tau \ . \qquad (18)$$

Here D is the diffusion coefficient, τ is the fluorescence lifetime of the excited state, and both θ and λ have been corrected for the index of refraction of the sample.

In all three samples, double exponential decays were observed. The fast component had a decay constant that was independent of θ and did not extrapolate to twice the fluorescence decay rate. Since this is not consistent with the predictions of Eq. (18), the mechanism causing this component is scattering from something other than a simple population grating. It is not particularly surprising that other mechanisms create an optical Kerr effect in a birefringent, ferroelastic crystal such as $Nd_xLa_{1-x}P_5O_{14}$, and these mechanisms will be studied in future experiments. The slower component of the double exponential decay had a decay constant that followed the predictions of Eq. (18) very closely and is therefore identified as being due to scattering from an excited-state population grating. It is this component of the total decay constant that is of interest in characterizing spatial energy migration.

TABLE I. Exciton diffusion parameters in $Nd_xLa_{1-x}P_5O_{14}$ crystals.

x	τ (μsec)	D (cm^2/sec)	l_a (μm)
0.2	294	5.2×10^{-7}	0.18
0.6	174	2.5×10^{-6}	0.30
1.0	124	5.1×10^{-6}	0.36

The decay constant K is plotted versus $\sin^2(\theta/2)$ in Fig. 3. With each sample, it is seen that K varies linearly with $\sin^2(\theta/2)$ and extrapolates to twice the fluorescence decay rate for $\theta=0$ as predicted by Eq. (18). By calculating the slope of the theoretical fit to the data, Eq. (18) can be used to obtain the diffusion coefficient D. Table I lists the values of D determined for the three samples. These are for energy migration along approximately the crystallographic a direction. It was more difficult to obtain data along other crystallographic directions due to higher background scattering, but in the $Nd_{0.2}La_{0.8}P_5O_{14}$ sample the diffusion coefficient along the b direction was found to be the same as along the a direction within experimental error.

The exciton migration length in the grating direction l_i can be defined as $l_i=\sqrt{2D\tau_0}$. The values obtained for l_i are listed in Table I.

In order to identify the microsopic interaction causing the exciton migration, the concentration dependence of the diffusion coefficient must be ascertained. For a random walk resulting from electric dipole-dipole interaction[16]

$$D=\{\tfrac{1}{2}[(4\pi/3)N_{so}]^{4/3}R_0^6/\tau_0\}x^{4/3} \ , \qquad (19)$$

where R_0 is the critical interaction distance, τ_0 is the intrinsic fluorescence lifetime, N_{so} is the concentration of ions on the exciton lattice for NdP_5O_{14}, and x is the normalized Nd concentration. Figure 4 shows a plot of D vs $x^{4/3}$. The linear variation of D with $x^{4/3}$ is consistent with Eq. (19). The use of values of $\tau_0=350$ μsec and $N_{so}=4\times10^{21}$ cm^{-3} and fitting the data in Fig. 4 with Eq. (19) gives a value of $R_0=45$ Å. This long-range interaction distance will overcome any crystal anisotropy which is consistent with the observation that the diffusion coefficient is the same along the a and b directions.

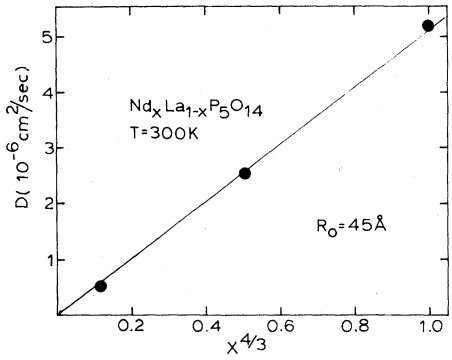

FIG. 4. Concentration dependence of the exciton diffusion coefficient at room temperature.

Next, it is important to determine the role played by the exciton migration in the concentration quenching properties of the material. The quenching rate is given by

$$W_Q=\tau^{-1}-\tau_0^{-1}\ , \tag{20}$$

where τ is the measured fluorescence decay time and τ_0 is the intrinsic fluorescence lifetime in the absence of concentration quenching. Again taking $\tau_0=350$ μsec the fluorescence lifetime and quenching rate plotted versus concentration in Fig. 5. At high concentrations the quenching rate varies linearly with concentration as shown in Fig. 5. This linear concentration dependence of the quenching rate together with the long exciton migration lengths listed in Table I indicate that the dominant quenching process in the higher concentration $Nd_xLa_{1-x}P_5O_{14}$ crystals is an exciton diffusion and trapping mechanism. At low concentrations the quenching rate no longer varies linearly with concentration as can be seen in Fig. 5. This region is expanded in Fig. 6 where the quenching rate is plotted both versus concentration and the square of the

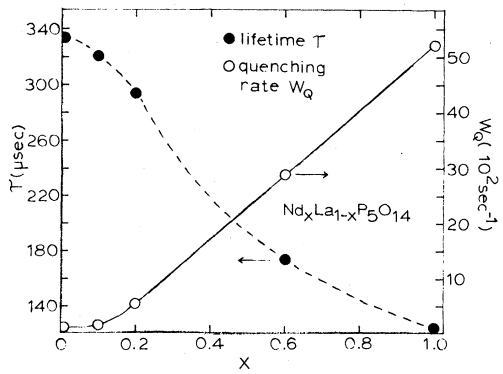

FIG. 5. Concentration dependence of the fluorescence lifetime and quenching rate at room temperature.

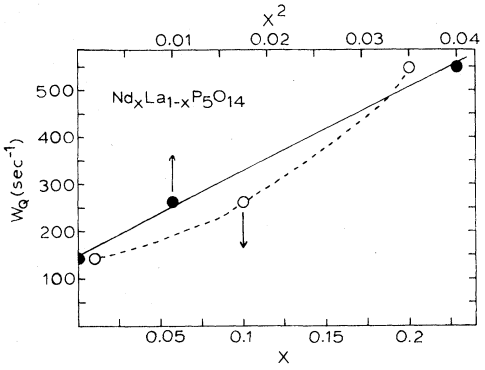

FIG. 6. Concentration dependence of the quenching rate at room temperature for samples with low Nd concentrations.

concentration for the three samples with smallest values of x. It is seen that for these low-concentration samples, the quenching rate varies approximately quadratically with concentration, which is consistent with an ion pair cross-relaxation quenching mechanism.

V. SUMMARY AND CONCLUSIONS

Three important results have been described in the preceding sections. The first is the derivation of the expression describing the intensity of the FWM signal beam in the typical configuration used for studies of exciton dynamics. This shows the effects of not having the beams exactly phase matched and the instabilities that arise for very small write beam crossing angles. The latter effect was encountered experimentally. The second is the demonstration that excitons diffuse over an average distance of 0.36 μm in a specific direction in NdP_5O_{14} at room temperature. The third is the implication obtained from the concentration dependence of the fluorescence quenching that at very low concentrations quenching occurs through cross relaxation while at high concentrations the quenching mechanism is exciton migration to sinks.

There has been significant controversy in the literature concerning the concentration quenching mechanism in stoichiometric laser materials and whether exciton diffusion occurs in these materials or not. The arguments on these subjects have been discussed elsewhere and will not be repeated here.[4,17] Some of the discrepancies in data reported previously may be due to differences in sample quality since it has only been recently that it has been possible to obtain good single crystals of large size and high optical quality.[13]

The results reported here showing that different quenching mechanisms are active in high- and low-concentration samples are consistent with the observed differences of the effects of high pressure on the optical spectra of stoichiometric rare-earth materials.[18] The exponential shape of the population grating FWM signal decay indicates that exciton motion is diffusive at room temperature.[6,11] The nature of the trapping sites and quenching interaction has not yet been determined. The sample surface has been shown to play some role in the quenching but it does not appear to be the dominant quenching site.[5] Also it is important to note that hydroxyl radicals which were known to cause quenching in early materials of this type are not present in the high quality samples used in this study.

The observation of long-range exciton diffusion in NdP_5O_{14} at room temperature is consistent with the recent low-temperature photon-echo results obtained on similar EuP_5O_{14} crystals which show the excitons to be delocalized.[19] Attempts are currently underway to repeat these FWM experiments at low temperatures to determine the role played by phonons in the exciton migration and trapping process. However, additional experimental complications such as added background scattering from dewar windows and reduced absorption of the signal beams have so far inhibited low-temperature measurements of this type. These will be pursued further in the future as well as additional investigations into the nature of the unexplained angular-independent scattering mechanism.

ACKNOWLEDGMENTS

This work was supported by the U.S. Army Research Office and National Science Foundation Grant No. DMR-7916152.

[1]C. M. Lawson, R. C. Powell, and W. K. Zwicker, Phys. Rev. Lett. 46, 1020 (1981).
[2]H. G. Danielmeyer, in *Festkörperprobleme,* edited by H. J. Queisser (Pergamon, New York, 1975), Vol. 15, p. 253.
[3]H. P. Weber, Opt. Quantum Electron. 7, 431 (1975).
[4]J. M. Flaherty and R. C. Powell, Phys. Rev. B 19, 32 (1979).
[5]R. C. Powell, D. P. Neikirk, J. M. Flaherty, and J. G. Gualtieri, J. Phys. Chem. Solids 41, 345 (1980).
[6]J. R. Salcedo, A. E. Siegman, D. D. Dlott, and M. D. Fayer, Phys. Rev. Lett. 41, 131 (1978).
[7]A. Yariv and D. M. Pepper, Opt. Lett. 1, 16 (1977).
[8]A. E. Siegman, J. Opt. Soc. Am. 67, 545 (1977).
[9]R. L. Abrams and R. C. Lind, Opt. Lett. 2, 94 (1978); 3, 205 (1978).
[10]P. F. Liao and D. M. Bloom, Opt. Lett. 3, 4 (1978).
[11]V. M. Kenkre, Phys. Rev. B 18, 4064 (1978); Y. M. Wong and V. M. Kenkre, *ibid.* 22, 3072 (1980); V. M. Kenkre, Phys. Lett. A 82, 100 (1981).
[12]H. Kogelnik, Bell Sys. Tech. J. 48, 2909 (1969).
[13]R. D. Plattner, W. W. Kruhler, W. K. Zwicker, T. Kovats, and S. R. Chinn, J. Cryst. Growth 49, 274 (1980).
[14]A. Yariv, *Quantum Electronics* (Wiley, New York, 1975), p. 149.
[15]C. M. Lawson, doctoral dissertation, Oklahoma State University, 1981 (unpublished).
[16]Th. Förester, Ann. Phys. 2, 55 (1948).
[17]W. Lenth, G. Huber, and D. Fay, Phys. Rev. B 23, 3877 (1981); D. Fay, G. Huber and W. Lenth, Opt. Commun. 28, 117 (1979).
[18]L. D. Merkle, I. L. Spain, and R. C. Powell, J. Phys. C 14, 2027 (1981).
[19]R. M. Shelby and R. M. Macfarlane, Phys. Rev. Lett. 45, 1098 (1980).